Theory of magnetoconductivity in a two-dimensional electron-gas system: Self-consistent screening model

Yoshimasa Murayama
Advanced Research Laboratory, Hitachi, Limited, Kokubunji, Tokyo 185, Japan

Tsuneya Ando
Institute for Solid State Physics, University of Tokyo, 7-22-1 Roppongi, Minato-ku, Tokyo 106, Japan
(Received 14 April 1986)

Transverse magnetoconductivity σ_{xx} is investigated for a two-dimensional electron-gas (2D EG) system in magnetic fields. A scattering model commonly applicable to both Si metal-oxide-semiconductor (MOS) and $Al_xGa_{1-x}As$-GaAs heterostructure field-effect transistors (FET's) is investigated. Ionized impurities are taken to exert a Coulomb force which is screened by the 2D EG. The screened Coulomb force determines widths of Landau subbands and, hence, the density of states at the Fermi energy in Landau subbands, which specifies the degree of screening. Thus, when calculating the widths, broadening of subbands and static dielectric response (i.e., screening) are considered self-consistently (self-consistent screening model). Both widths and σ_{xx} are solved analytically as well as numerically. Calculations are carried out both when impurities exist within the 2D EG and when they are in a remote sheet. Calculated σ_{xx} is compared with the experiment by Narita *et al.* and good agreement, though qualitative, is obtained. The real-space behavior of the screened potential is also discussed. The force range becomes short or remains long, depending on the degree of screening.

I. INTRODUCTION

In a series of papers[1-4] (for a review, see Ref. 5) magnetoconductive properties of Si metal-oxide-semiconductor field-effect transistors (MOSFET's) have been studied and the basic concept in understanding them was constructed on a δ-function-type scattering potential, i.e., an extremely short-range potential. Along with this theory[1-4] most theories of conduction in two- and three-dimensional (2D or 3D) electron gas (EG) in magnetic fields use a Gaussian potential due to ease of handling. The potential is advantageous for analytical study in terms of force range.

Throughout the present study the nature of force range is always considered. The most effective way to determine it is thought to be the screening effect. As is commonly accepted nowadays, one of the most dominant scatterings in MOSFET's and heterostructure devices is due to ionized impurities, however near or far from 2D EG they exist, so long as the density of carriers is at low levels. Since only low-temperature properties are of present concern in this study, phonon scatterings play a minor role.

The screening effect in 3D magnetoplasma has been discussed by several authors.[6-8] For a 2D EG in magnetic fields, screening was first precisely investigated in ionized impurity scattering by one of the present authors (T.A.).[9,10] In particular, the importance of a self-consistent treatment in such a problem was stressed.[10]

The calculational scheme of dielectric response in Ref. 9 assumes that scattering is of an extremely short-ranged nature. Then the damping of an electron, Γ, is always independent of the Landau quantum number N, which makes it easy to calculate the response, taking all subbands into account. After completing the formulation, Γ is replaced by Γ_N. The scheme was applied to studying cyclotron resonance widths and σ_{xx}.[10]

Following this idea Das Sarma[11] discussed self-consistent Landau subband widths in the quantum limit. Lassnig and Gornik[12] also solved self-consistent cyclotron resonance widths using the formulas given in Ref. 9.

The point of self-consistent screening in a 2D EG under magnetic fields is as follows. A Landau quantized 2D EG gives a series of discrete but broadened subbands due to several scattering mechanisms. If the Fermi level is situated within a gap region between two neighboring subbands and, hence, every nonoverlapping subband is completely occupied or unoccupied, it is intuitively understood that no carriers are mobile and there cannot occur any reallocation of carriers causing screening within a single subband.

As for intersubband terms they do not contribute to screening, at least in the limit of vanishing momentum transfer, $\mathbf{q}\rightarrow\mathbf{0}$. Thus the "bare" Coulomb potential still remains unscreened.

On the other hand, maximum screening occurs when the density of states (DOS) at the Fermi level is maximal, that is, when the Fermi level is at the center of a symmetrical subband. When a single scattering origin, i.e, ionized impurity scattering is assumed to exist, broadening features are determined by the Coulomb potential whose manner of screening is determined by the broadening.

This kind of exact self-consistency in screening was first applied to a 2D EG apart from impurities.[13] When subband and cyclotron widths are calculated, they become very broad for Fermi levels lying between subbands.[10,13]

Since extraordinary broadening occurs in that case, some overlap of subbands certainly results. The effect limits the widths to grow infinitely and reasonable widths can be calculated.[14]

In this paper, self-consistency is pursued extensively within a single subband approximation. Special attention is placed on analytical solutions of self-consistent equations.

In this model how σ_{xx} behaves as a function of Landau quantum number N is one of the main subjects of interest. For an extremely short-range potential an important result[1] is that peak values in σ_{xx} are expressed by a universal constant, $(N+\frac{1}{2})e^2/\pi^2\hbar$, where e is the electronic charge and $\hbar$ the Planck constant per 2π. It is interesting to see how the peaks behave when a potential is not assumed *a priori* to be extremely short ranged but is specified by screening.

Dopants sometimes exist in a remote region from the 2D EG. It is also interesting to understand conductive properties when scatterers exist outside a channel.[13] As is seen in Fig. 1, the peaks in σ_{xx} do not increase with N, but rather decrease. It is easy to show that for a Gaussian potential with a constant, long potential range d such as $d \gg l$ [l the cyclotron radius, equal to $(\hbar/eB)^{1/2}$], peak values do not increase with N but are almost constant.[15] However, it is quite difficult to understand why the same screened Coulomb potential is short ranged in Si MOSFET's (Refs. 16 and 17) and long ranged in heterostructure devices,[18–20] so long as impurities are similarly present within 2D EG. The difference seems to come from the fact that impurities in Si MOSFET's exist just at the Si-SiO_2 interface, whereas in GaAs-$Al_xGa_{1-x}As$ devices they are present only outside a channel. Since at the GaAs-$Al_xGa_{1-x}As$ interface both semiconductor layers are grown successively and heteroepitaxially during a single batch process, it is certainly believed that this system induces few ionized centers. Here we aim at affirming whether remote impurities exert a "long-ranged" potential on 2D EG.

The structure of this paper is as follows. First the screening effect due to 2D Landau electrons is considered. Next, σ_{xx} is calculated using Kubo's $\dot{X}$-$\dot{X}$ correlation formula.[21,22] Assuming that $\omega_c\tau \gg 1$, a single subband approximation is justified. The behavior of the screened Coulomb potential in real space is eventually discussed after a self-consistent potential has been calculated in its Fourier transform. A part of this work has already been reported.[23]

II. MODEL AND FORMALISM

We start from Dyson equations for a Landau state as shown in Fig. 2. Each heavy solid line, i.e., the propagator of a Landau electron G, includes a repetition of the self-energy part Σ. Σ is composed of scattering events by impurities. All kinds of crossed diagrams are discarded from the start for simplicity. If one is aiming at a discussion of localized states or multiple scattering by a single impurity with a long-range potential, crossed diagrams seem to play an important role.[24] Here only extended states are of concern. The peaking structure in σ_{xx} implies that the extended character of Landau states carries the whole current.[25]

A bare Coulomb potential is screened, as is shown by the wavy lines in Fig. 2. The polarizability Π includes a vertex correction V, which is also expressed by a Dyson equation in the figure. The transverse magnetoconductivity is given by an $\dot{X}$-$\dot{X}$ correlation function.[21,22] As has been considered,[1] the $\dot{X}$-$\dot{X}$ correlation implicitly includes all orders of ladder-type interaction between two propagators, as suggested at the bottom in Fig. 2. Hence, the same vertex correction (i.e., all the higher-order terms appearing in σ are summed up giving the same vertex correction) should be precluded in the $\dot{X}$-$\dot{X}$ diagram. (The double dashed lines therein stand for the $\partial v/\partial y$ interaction, instead of the v interaction, which has two wavy lines on both sides.) The replacement of the j-j correlation by the $\dot{X}$-$\dot{X}$ correlation within a single subband is jus-

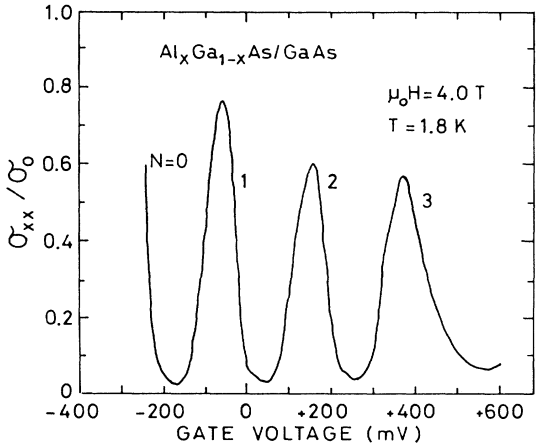

FIG. 1. Observed transverse magnetoconductivity σ_{xx} versus gate voltage in an $Al_xGa_{1-x}As$-GaAs heterostructure FET. $\sigma_0=e^2/\pi^2\hbar$. After Narita (Ref. 18).

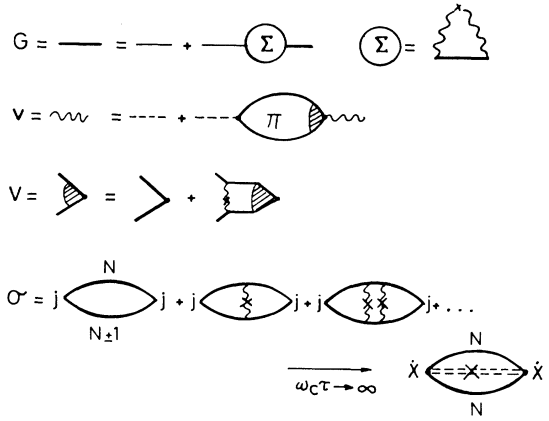

FIG. 2. Diagrammatic equations for Landau electrons considered in this study.

tified in the limit of $\omega_c\tau\rightarrow\infty$.

Following a textbook such as that of Abrikosov *et al.*,[27] we easily proceed to obtain final equations in explicit forms. Two assumptions are the following.

(i) All coupling between different quantum numbers is neglected. Hence, the Green's function $V_{NN'}$ is taken to be diagonal. This is justified when $\omega_c\tau\gg1$. There, higher Landau subbands are well separated, and the mixing of states with different quantum numbers is considered to be negligibly small.

(ii) Temperature is assumed to be 0 K.

From translational symmetry, all Green's functions are independent of X, the quantum number corresponding to the coordinate of the center of cyclotron motion.

The Coulomb interaction between electrons and ionized impurities, which are randomly distributed, is effectively expressed as follows:[22]

$$\langle \tilde{U}(\mathbf{q},z)^*\tilde{U}(\mathbf{q}',z)\rangle_S = L^{-4}\sum_{i,j}\langle e^{i\mathbf{q}\cdot\mathbf{R}_i-i\mathbf{q}'\cdot\mathbf{R}_j}\rangle_{ij} v(\mathbf{q},z)^*v(\mathbf{q}',z) = n_i L^{-2}\,|\,v(\mathbf{q},z)\,|^2\delta_{\mathbf{q}\mathbf{q}'}\ , \tag{2.1}$$

where $U(\mathbf{r})$ is $\sum_j v(\mathbf{r}-\mathbf{R}_j)$ and its Fourier transform $\tilde{U}(\mathbf{q},z)$ reads $L^{-2}\sum_j e^{-i\mathbf{q}\cdot\mathbf{R}_j}v(\mathbf{q},z)$. All variables are two dimensional and n_i is the 2D density of impurities. z is the coordinate of an impurity in the direction perpendicular to the 2D EG. Throughout this study a $\delta(z-z_j)$-shaped profile of impurities is assumed for clarity. $\langle\cdots\rangle_S$ means an average over randomly distributed scatterers' 2D variables: $(\mathbf{R}_{xj},\mathbf{R}_{yj})$. The distribution is assumed homogeneous and no coherence is considered between scattering events (Born approximation). L is a dimension within which the system is quantized. The random variable $\mathbf{R}_j$ stands always within $(z=0)$ or in a remote sheet $(z\neq0)$ from the 2D EG. In the equation

$$\langle NX\,|\,U(\mathbf{r})\,|\,N'X'\rangle = L^{-2}\sum_{\mathbf{q},j}e^{-i\mathbf{q}\cdot\mathbf{R}_j}v(\mathbf{q},z)\langle NX\,|\,e^{i\mathbf{q}\cdot\mathbf{r}}\,|\,N'X'\rangle\ , \tag{2.2}$$

the matrix element

$$\langle NX\,|\,e^{i\mathbf{q}\cdot\mathbf{r}}\,|\,N'X'\rangle = \exp[il\mathbf{q}_x(X/l+l\mathbf{q}_y/2)+i(N'-N)(\phi-\pi/2)]J_{NN'}(q)\delta_{X'-X,l^2\mathbf{q}_y} \tag{2.3}$$

is easy to obtain in terms of $\tan\phi=\mathbf{q}_y/\mathbf{q}_x$. $l=(\hbar/eB)^{1/2}$. $J_{NN'}(q)$ is given in Appendix B. The phase factor in Eq. (2.3) plays an important role when a vertex correction is calculated.

First of all, utilized formulas are listed. The Green's function $G_N(E)$ is given by the following Dyson equation:

$$\Sigma_N(E)=(\Gamma_N^2/4)G_N(E)\ , \tag{2.4}$$

where Γ_N is defined by

$$\Gamma_N^2/4=(n_i/2\pi)\int dq\,q\,|\,v(\mathbf{q},z_i)\,|^2[J_{NN}(q)]^2\ . \tag{2.5}$$

The screened Coulomb interaction $v(\mathbf{q},z_i)$ is[28]

$$v(\mathbf{q},z_i)=V_0\exp(-q\,|\,z_j\,|\,)/[q+V_0\Pi_N(q)]\ ,\qquad V_0=2\pi e^2/\kappa\ , \tag{2.6}$$

where κ is an effective static dielectric constant. As is expressed in Fig. 2, $\Pi_N(q)$ is calculated as

$$\Pi_N(q)=\{[J_{NN}(q)]^2/2\pi^2l^2\}\times\int dE\,f(E)\mathrm{Im}[G_N^2/(1-B_N(q)G_N^2)]\ , \tag{2.7}$$

where $f(E)$ is the Fermi-Dirac distribution function. In the above equation,

$$B_N(q)=(\Gamma_N^2/4)F_N(q) = (n_i/2\pi)\int dq'\,q'J_0(l^2qq')\,|\,v(\mathbf{q}',z_i)\,|^2\times[J_{NN}(q')]^2 \tag{2.8}$$

implies an effect of vertex correction. $J_0(l^2qq')$ is the Bessel function of zeroth order and should not be confused with the J_{NN} function. In Appendix A a more detailed derivation of this equation is described. The effect of the vertex correction will be discussed in the following section.

The solution of the Dyson equation (2.4),

$$\Sigma_N=\tfrac{1}{2}(E-\varepsilon_N)+i\tfrac{1}{2}\Gamma_N\{1-[(E-\varepsilon_N)/\Gamma_N]^2\}^{1/2}\ , \tag{2.9}$$

is used hereafter. The full width equals $2\Gamma_N$.

For convenience these equations are rewritten in normalized form. The normalization for energy is $E_c=e^2/\kappa l$, and the variable q is transformed into x by $x=(ql)^2/2$. Then from Eqs. (2.4)–(2.8),

$$\Gamma_N^2/4E_c^2=c^{-1}=(c_i/2)\int dx\,[J_{NN}(x)]^2e^{-2\sqrt{2x}\,|z_i|/l}/[\sqrt{x}+\bar{s}(x)]^2\ , \tag{2.10}$$

$$F_N(x)=(cc_i/2)\int dy\,J_0(2\sqrt{xy})[J_{NN}(x)]^2e^{-2\sqrt{2x}\,|z_i|/l}/[\sqrt{y}+\bar{s}(y)]^2\ , \tag{2.11}$$

and

$$\bar{s}(x)=(lV_0/\sqrt{2})\Pi_N(q)=(c/2\pi^2)^{1/2}[J_{NN}(x)]^2\int d\varepsilon\,f(\varepsilon)(-\varepsilon)[1-(\varepsilon/2)^2]^{1/2}/[(F_N+1)^2-F_N\varepsilon^2] \tag{2.12}$$

are obtained. $F_N(0)=1$ is obvious.

c_i is a parameter to describe the average number of impurities within the cyclotron radius, equal to $2\pi l^2$. The integra-

tion in Eq. (2.12) is from $\varepsilon_{\min}$ to ε_F. ε stands for $(E-\varepsilon_N)/E_c$. $\varepsilon_{\min}$ and ε_F are the minimum energy of the Nth subband and the Fermi level in the unit of E_c, respectively. The transverse magnetoconductivity σ_{xx} in terms of the $\dot{X}$-$\dot{X}$ correlation reads

$$\sigma_{xx}/\sigma_0=(cc_i/2)\int dxx\,[J_{NN}(x)]^2 e^{-2\sqrt{2x}\,|z_i|/l}/[\sqrt{x}+\bar{s}(x)]^2 . \tag{2.13}$$

Throughout this paper we are concerned only with the peak values in σ_{xx}, i.e., when the Fermi level stands at the peak position of each Nth subband. In this case the above integral (2.12) becomes simple. The solution will be discussed in the following section.

III. ANALYTICAL CONSIDERATIONS

A. Screening

In order to calculate the dielectric response, we start with Eq. (2.11), which expresses a contribution of the corrected vertex to the polarizability. So long as a single subband approximation is taken, only the zeroth-order Bessel function J_0 appears in the integral equation (2.11), which stems from the phase factor in Eq. (2.3) (cf. Appendix A).

First let us solve Eq. (2.12). The integral is given in an analytical form, when the Fermi level stands at one of the subband peaks. The calculation of Π_N in terms of F_N defined in Eq. (2.11) is straightforward.

(i) For positive F_N:

$$\Pi_N(x)=\sqrt{2\bar{s}}(x)/lV_0=D(\varepsilon_F)[J_{NN}(x)]^2\{1-[(1-F_N)/2\sqrt{F_N}]\arctan[2\sqrt{F_N}/(1-F_N)]\}/F_N . \tag{3.1}$$

(ii) For negative F_N:

$$\Pi_N(x)=\sqrt{2\bar{s}}(x)/lV_0=D(\varepsilon_F)[J_{NN}(x)]^2\{[(1+|F_N|)/2|F_N|^{3/2}]\ln[(1+\sqrt{|F_N|})/(1-\sqrt{|F_N|})]-1/|F_N|\} . \tag{3.2}$$

The function contained inside of the curly brackets in Eqs. (3.1) and (3.2) denoted as $\mathcal{F}_N$, is plotted in Fig. 3.

An approximate form of F_N in Eq. (2.8) is conceptually discussed in terms of force range d for a Gaussian-type potential.

(a) For a short-range potential ($d \ll l$),

$$F_N(q)\cong[J_{NN}(q)]^2 \tag{3.3}$$

is easily concluded, since $|v(\mathbf{q},z_i)|^2$ is roughly independent of $\mathbf{q}$. (See Appendix B.)

(b) For a long-range potential, i.e., $d \gg l$, cases should be classified into two groups according to $\mathbf{q}$ value.

$d \gg l$ and $d/l^2 \gg q$. We can approximate as $J_0 \cong 1$. Hence,

$$F_N(q)\cong 1 . \tag{3.4}$$

$d \gg l$ and $q \gg d/l^2 \gg 1/l$. Since J_0 in Eq. (2.8) oscillates markedly, the integral almost vanishes, i.e.,

$$F_N(q)\cong 0 . \tag{3.5}$$

Using this F_N, an asymptotic behavior of $\Pi_N(q)$ is calculated from Eqs. (2.7) and (2.8) when 0 K is assumed for temperature.

In case $F_N(q)\cong 1$, the calculation proceeds as follows:

$$\begin{aligned}\Pi_N(q)&=\{[J_{NN}(q)]^2/2\pi^2l^2\}\\&\quad\times\int dE\,f(E)\mathrm{Im}[G_N^2/(1-\Gamma_N^2G_N^2/4)]\\&=[J_{NN}(q)]^2D(\varepsilon_F) ,\end{aligned} \tag{3.6}$$

where the density of states is $D(\varepsilon_F)=\mathrm{Im}G_N(\varepsilon_F)/2\pi^2l^2=1/\pi^2l^2\Gamma_N$ and an identity $dG_N/dE=-G_N^2/(1-\Gamma_N^2G_N^2/4)$ is used. The latter relation easily results from differentiation of Eq. (2.4) along with $G_N^{-1}=E-\varepsilon_N-\Sigma_N$.

In case $F_N(q)\cong 0$, a rather complicated calculation follows. Using $X_N=G_N^{-1}$ and the relation, $dE/dX_N=1-\Gamma_N^2/4X_N^2$,

$$\begin{aligned}\Pi_N(q)&=(J_{NN}^2/2\pi l^2 2\pi i)\int_{\varepsilon_{F-}}^{\varepsilon_{F+}}dE\,X_N^{-2}\\&=J_{NN}^2\tfrac{4}{3}D(\varepsilon_F)\end{aligned} \tag{3.7}$$

reads, where $\varepsilon_{F\pm}=\varepsilon_F\pm i0$.

We next summarize the behavior of Π_N. Take the $N=0$ case for example. (See Fig. 4.)

(a) In the short-range scattering case, $F_0\cong J_{00}^2=\exp(-q^2l^2/2)$ varies from 1 for $q=0$ to 0 for $q\to\infty$. Π_0 traces the $\frac{4}{3}J_{00}^2D(\varepsilon_F)$ curve (short-wavelength limit) for $q \gg 1/l$ and then follows the $J_{00}^2D(\varepsilon_F)$ curve for $q \lesssim l^{-1}$, which we call the long-range limit, as will be discussed in (b).

(b) In the long-range scattering case, a sketch similar to

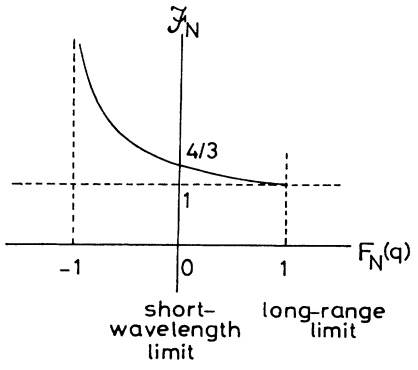

FIG. 3. Rough sketch of $\mathcal{F}_N$ vs F_N. The point of $F_N=0$ is the short-wavelength limit and $F_N=1$, the long-range limit.

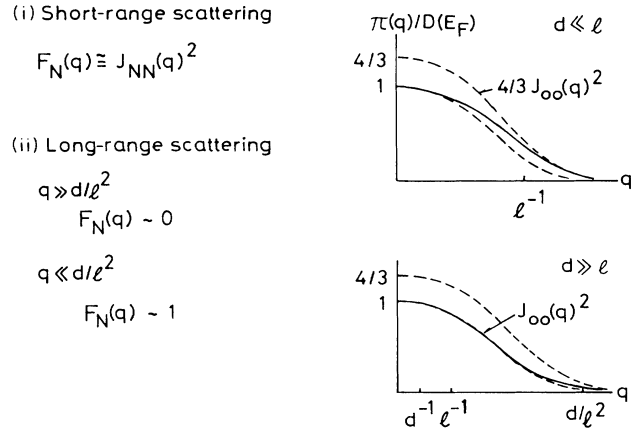

FIG. 4. Plots of polarizability $\Pi(q)$ normalized by the density of states $D(\varepsilon_F)$ [equal to $\mathscr{F}_0 J_{00}(q)^2$] versus q. d is a representative force range.

that shown above is possible. Within the region of $q \lesssim l^{-1}$, where J_{00}^2 has an appreciable magnitude, Π_0 always follows a curve of $J_{00}^2 D(\varepsilon_F)$. For $q \gg d/l^2$, it is given by $\frac{4}{3}$ as large as this, although J_{00} is quite small there. With this meaning $\Pi_0 = J_{00}^2 D(\varepsilon_F)$ is defined as the long-range limit (LR limit).

The fact that the polarizability Π_N is enhanced by a factor of $\frac{4}{3}$ is compatible with stronger screening, i.e., a shorter-range case. Thus it is safe to say that the effect on screening caused by force range is only by a factor of $\frac{4}{3}$. Or, since the width of subbands and σ_{xx} are proportional to $|v(\mathbf{q},z_i)|^2$, i.e., to the inverse square of Π_N, the effect is at most doubled. This point will be affirmed by numerical calculation in the following.

It is an elaborate task to numerically calculate Eqs. (2.11) and (2.12) self-consistently, using (3.1) and (3.2), without any approximation. In the simplest case with scatterers existing within 2D EG, the solution is obtained by iterative calculation and is shown in Fig. 5.

In Fig. 5 (a) full widths of Landau subbands equal to $2\Gamma_N$ are plotted as a function of Landau quantum number N of the subband of concern. In the parameter $c_i = 2\pi l^2 n_i$, n_i is the density of impurities. Also in Fig. 5(b) the peak values in σ_{xx} are plotted in a similar way. The triangles represent the values for the short-wavelength limit (i.e., when the polarizability has the factor $\frac{4}{3}$); the solid circles, the solutions for the short-range limit, i.e., $\Pi_N(q) = D(\varepsilon_F) J_{NN}(q)^2 \mathscr{F}_N$ with $\mathscr{F}_N$ evaluated for $F_N = J_{NN}(q)^2$; the open circles, the self-consistently numerically solved solutions and the crosses, the values for the long-range limit, i.e., $F_N(q) = 1$, or accordingly, $\Pi_N(q) = J_{NN}(q)^2 D(\varepsilon_F)$.

From Fig. 5(a) it is seen that the solutions with vertex correction self-consistently included always lie between the long-range limit solutions (LR limit, $\times$) and short-wavelength ones (SWL limit, $\triangle$). This is reasonable when Fig. 6 is examined, where the self-consistently solved $F_N(x)$ (lower curves) and $\mathscr{F}_N(x)$ (upper curves) are plotted. F_N is almost between 1 (LR limit) and 0 (SWL lim-

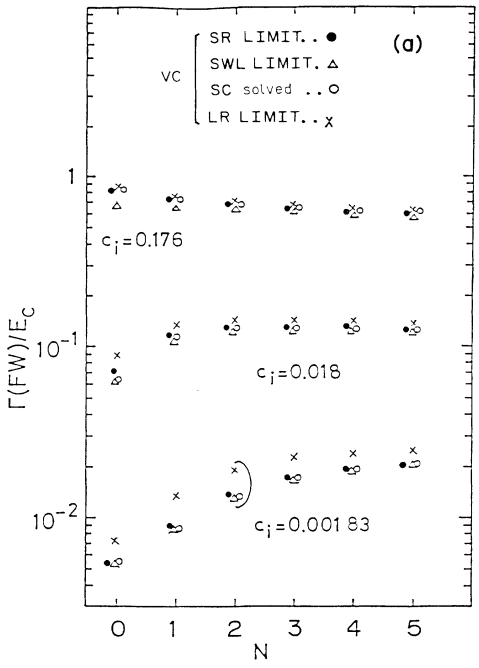

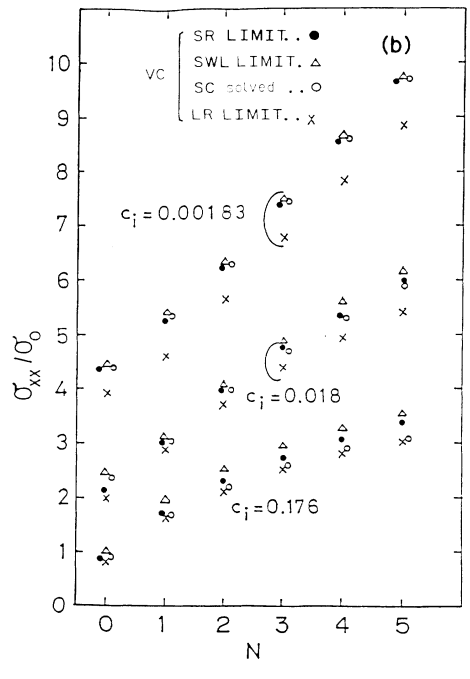

FIG. 5. Calculated (a) full widths of Landau subbands $2\Gamma_N$ normalized by $E_c = e^2/\kappa l$ and (b) peaks in σ_{xx} normalized by σ_0 versus Landau quantum number N. Impurities are assumed to exist within 2D EG. The crosses are for the long-range limit, the solid circles for the short-range limit, the open circles for the self-consistently solved widths, and the triangles for the short-wavelength limit. c_i is $2\pi n_i l^2$, where n_i is the 2D density of impurities. $n_i = 0.2418 c_i$ times (B in T) $\times 10^{11}/\text{cm}^2$.

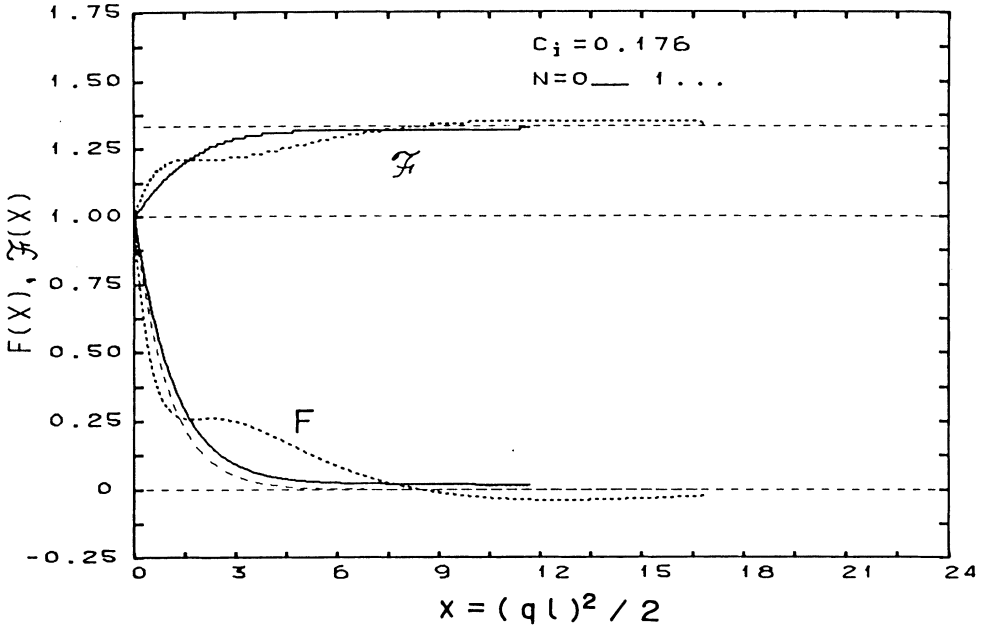

FIG. 6. Self-consistently solved $\mathcal{F}_N(x)$ (upper curves) and $F_N(x)$ (lower curves) versus $x=(ql)^2/2$ in the case of $c_i=0.176$. Solid lines are for $N=0$ and the dotted lines are for $n=1$. For comparison $F_0(x)=J_{00}(x)^2$ is plotted by a thin dashed line in the lower part, which is the short-range limit solution.

it), which implies that it is between both limits, whereas $\mathcal{F}_N$ defined by $\Pi_N(x)/D(\varepsilon_F)[J_{NN}(x)]^2$ is between 1 (LR limit) and $\frac{4}{3}$ (SWL limit).

As is seen in Fig. 5, the self-consistent solutions almost coincide with those in the short-range limit, except when c_i is large (0.176). Thus for large c_i's, scattering seems considerably long ranged.

When $n_i(c_i)$, or accordingly, the subband width is small, screening is very effective because of a large peak DOS. Strong screening implies a short-range nature of the scattering potential. Thus lower points in Fig. 5(a) [a small $n_i(c_i)$] show short-range characteristics. The corresponding σ_{xx} behaves as do the upper points in Fig. 5(b). As is the case for an extremely short-range potential calculation,[1] σ_{xx} grows as a function of N, as $(N+\frac{1}{2})\sigma_0$ with $\sigma_0=e^2/\pi^2\hbar$. The present self-consistent solutions are roughly several times as large as $(N+\frac{1}{2})\sigma_0$ (10 times for $N=0$ and 1.8 times for $N=5$).

As for a large $n_i(c_i)$, the dependence of the width on N is highly alleviated compared to the above-mentioned small $n_i(c_i)$ cases. The σ_{xx} has a rather insensitive dependence on N. This insensitivity is a marked feature for a long-range potential.[15] The analytical dependence on c_i of widths and peaks in σ_{xx} will be investigated in the following section.

Since it has been clarified that the self-consistent inclusion of the vertex correction does not drastically change the behavior of physical quantities of present concern, we will henceforth always treat problems in the *long-range limit,* i.e., with the polarizability taken to be $\Pi_N=J_{NN}^2D(\varepsilon_F)$ and, therefore, $F_N(x)=1$.

B. Self-consistent solutions

It seems instructive to find analytical solutions to the self-consistent equation. We reproduce Eq. (2.10) for $N=0$ again:

$$\int_0^\infty dx(2c_i/\gamma_0^2)e^{-x-2\sqrt{x}z}/(\sqrt{x}+be^{-x})^2=1\ , \qquad (3.8)$$

with $b=\sqrt{2}/\pi\gamma_0$. $\gamma_0=\Gamma_0/E_c$ is the normalized width of the 0th subband and $z=\sqrt{2}z_i/l$. The equation for σ_{xx} reads

$$\sigma_{xx}/\sigma_0=\pi^2b^2c_i\int dx\, xe^{-x-2\sqrt{x}z}/(\sqrt{x}+be^{-x})^2\ . \qquad (3.9)$$

The integrand in Eq. (3.8), denoted as $f(x)$, has a form not easily approximated. If the second term in the denominator is neglected for $x\to\infty$, the integral actually diverges logarithmically. $f(x)$ is plotted in Fig. 7 for $c_i=0.002$, 0.018, and 0.176, when $z=0$. When c_i is small (e.g., $c_i=0.002$ shown by the solid line in Fig. 7), the integral has its main contribution from the region with nonvanishing q. As a result, the potential is oscillatory in real space with a frequency $q_{\max}$, where the integrand becomes maximal. In addition, in the meaning that the potential is finite over a wide range of q, it seems rather like short ranged. On the other hand, for $c_i=0.176$ (the dashed-dotted line in the figure) the potential decays rapidly with q; that is, the force range is long and the screening is weak.

We investigate analytically three cases classified by the values of c_i and z.

(i) For $c_i\ll 1$ with such an arbitrary z as $\sqrt{X}\gg z$, and

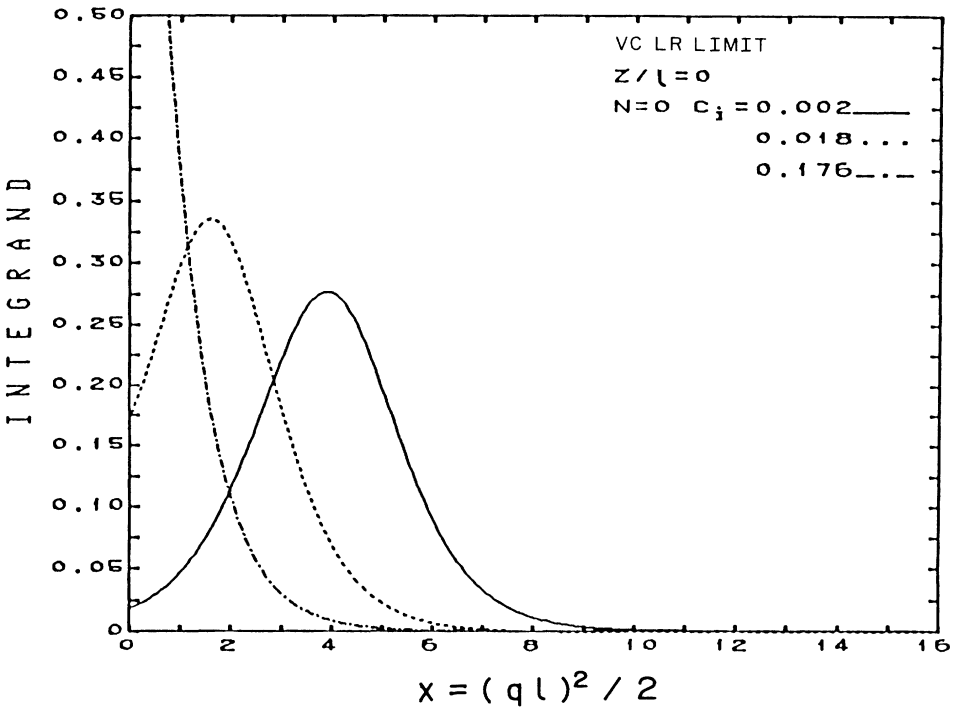

FIG. 7. Integrand of Eq. (3.8) versus $x=(ql)^2/2$. The vertex correction meets the long-range limit. The solid, the dashed, and the dashed-dotted lines are for $c_i=0.002$, 0.018, and 0.176, respectively. Impurities are assumed to exist within 2D EG (i.e., $z_i=0$).

(ii) for $c_i \gg 1$ with $z^2 \gg \pi^2 c_i/2$. Both cases have a large b and, hence, a large X.

The region of integration is divided in 2 in these cases: $[0,X)$ and $[X,\infty)$. X is the solution of $\sqrt{X}=b\exp(-X)$. $X \gg 1$ follows for a large b, and accordingly, a small γ_0. In the first region $\sqrt{x}$ is neglected in the denominator and the integration is simple, although not reproduced here.

For the other region, the second term in the denominator is neglected. The integral is given under the assumption of $\sqrt{X} \gg z$. The integration for σ_{xx} is similarly executable.

The final forms read

$$\gamma_0 \cong (\sqrt{8}\pi c_i/|C|)|(z^2+C)^{1/2}-z|e^{-2z[z+(z^2+C)^{1/2}]} \tag{3.10}$$

and

$$\sigma_{xx}/\sigma_0 \cong 2z^2+C+2z(z^2+C)^{1/2}-\pi^2 c_i/2\ , \tag{3.11}$$

where $C=-\ln(2\pi^2 c_i)$.

These expressions are valid also for a large z such as $z^2 \gg \pi^2 c_i/2$ along with $c_i \gg 1$ (ii). Seeing that $\ln c_i$ is rather insensitive to c_i, it is safe to say that the normalized width of the 0th subband, γ_0, is proportional to c_i and σ_{xx} depends little on c_i under these conditions. As for a large z, the width decreases as $\exp -4z^2$ and σ_{xx} increases as $4z^2$ with z.

This rapid decrease in width was already suggested in Ref. 13. It is a kind of "phase transition," which is caused by a positive feedback characteristic of the width as functions of c_i and $z=\sqrt{2}z_i/l$; this is quite a natural outcome of the self-consistent screening model. It was actually shown in Ref. 13 that Landau width becomes drastically narrow for impurities apart from the channel, by around 100 Å, under a reasonable doping condition.

(iii) For $c_i \gg 1$ with $z \ll 1$. This case has a small b and, hence, a small X.

Calculating procedures are very similar to (i) and (ii). Under the assumption of $1 \gg \sqrt{X} \gg 2z$, we obtain

$$\gamma_0 \cong (2c_i \ln\{[\pi(\alpha-\sqrt{\pi}z)]^2 c_i\})^{1/2} \tag{3.12}$$

and

$$\sigma_{xx}/\sigma_0 \cong 2c_i(1-\sqrt{\pi}z)/\gamma_0^2\ , \tag{3.13}$$

where $\alpha=1.2346$. In this case γ_0 is proportional to $c_i^{1/2}$. σ_{xx} is a logarithmic function of c_i, as was so in (i) and (ii).

The case with $\sqrt{X} \ll 1 \ll z$ does not appear, whose occurrence is physically difficult. Here it might help ones understanding to say a little about X. Take c_i to be 10^{-3}, for example. By solving the transcendental equation, $\sqrt{X}=be^{-X}$, and Eq. (3.10) for $z=0$, X becomes no more than ~ 5.3. Since we use an expansion formula such as $-\mathrm{Ei}(-X)=e^{-X}(1/X-1/X^2+\cdots)$ to reach the asymptotic solutions in (i) and (ii), $c_i=10^{-3}$ is still large for a limit like $X \gg 1$. This point will be discussed further in comparison with numerical solutions later.

It is desirable to calculate γ_0 and σ_{xx} for N's other than 0, but because of the complicated behavior of J_{NN} for $N \neq 0$, the task is formidable. We are satisfied with numerical solutions in the following section.

IV. NUMERICAL SOLUTIONS

A. σ_{xx}—impurities within 2D EG

We now proceed to a numerical calculation of Γ_N and σ_{xx}, when ionized impurities are assumed to exist within 2D EG. That is, z_i is zero in Eqs. (2.10)—(2.12). Polarizability is given in the long-range limit, as was discussed in the preceding section: $\Pi_N(x)=D(\varepsilon_F)J_{NN}(x)^2$.

Figure 8(a) shows calculated subband full widths $2\Gamma_N$ normalized by $E_c=e^2/\kappa l$, as a function of $c_i=2\pi n_i l^2$. As for GaAs ($\kappa=13.1$) and $B=20$ T, E_c is 19.2 meV and

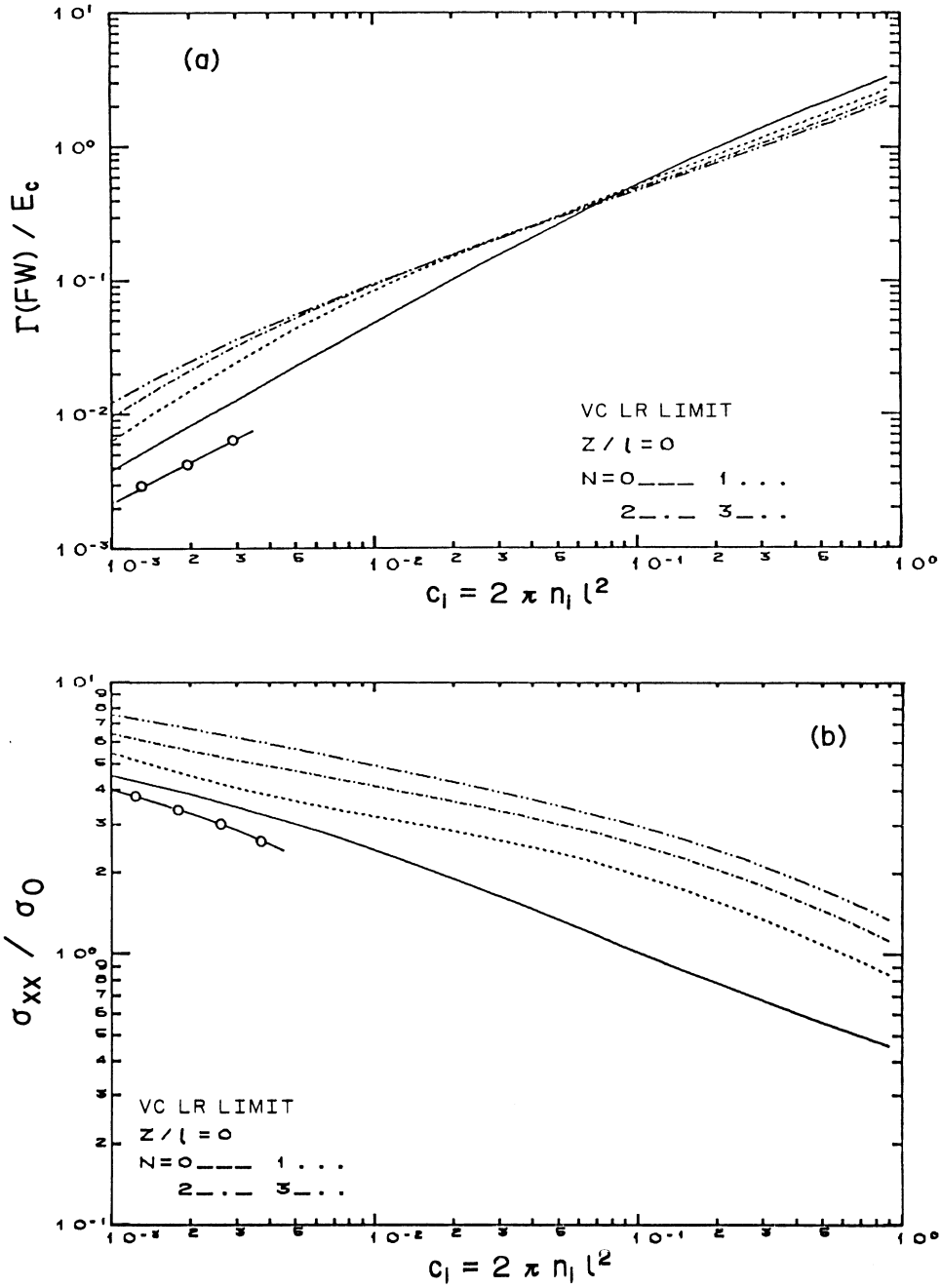

FIG. 8. Calculated (a) full widths of subbands, $2\Gamma_N$, normalized by $E_c=e^2/\kappa l$ and (b) peaks in σ_{xx} normalized by σ_0 vs $c_i=2\pi n_i l^2$ for $z_i=0$. The solid, dotted, dashed-dotted, and the dashed-double-dotted lines are for $N=0$, 1, 2, and 3, respectively. The horizontal axis scales to n_i by multiplying $48.3\times10^{10}/\text{cm}^2$ when $B=20$ T. The vertex correction is taken to be the long-range limit. The (-0-) curve is the asymptote in the small-c_i limit for $N=0$.

$\hbar\omega_c = 35.6$ meV. This relation of magnitudes justifies single subband approximation. It is seen in the figure that widths depend on N. The $N=0$ line is almost proportional to c_i in the small c_i region; it is parallel to the asymptote [Eq. (3.10) for $z=0$] plotted with a -0- line.

The region with large c_i's, where the asymptote derived previously is valid, is out of the scope of the figure. However, it is seen that the cases from $N=1$ through 3 appear to have a slightly smaller dependence on c_i, which suggests a closer affinity to the analytical solution, $\gamma_0 \propto (c_i \ln c_i)^{1/2}$ [Eq. (3.12)].

Figure 8(b) is for self-consistently solved peak values in σ_{xx}/σ_0. Regarding the variation with N the ratio of the Nth to the $(N+1)$th peak is approximately constant, except for $N=0$ in the large-c_i region. An analytically solved σ_{xx} claimed its rather insensitive dependence on c_i: $\sigma_{xx} \propto \ln(1/c_i)$. [Although Fig. 8(b) may at first sight seem to depend highly sensitively on c_i, one must be careful that the range of variation in σ_{xx}/σ_0 spans only one decade, whereas the horizontal axis spans three orders of magnitude.] The result that σ_{xx} varies with c_i stems from the self-consistent screening treatment within the scope of single subband approximation. Here self-consistency between the screening due to polarizable carriers and their subband width is too strictly taken into account.

Using the values in Fig. 8(a) it is possible to discuss parameter-dependent subband widths. Since in our model σ_{xx} peaks depend on B and n_s through their c_i dependence, they behave differently in experiment when it is performed for either the B or n_s parameter. This was pointed to in Ref. 23. When an experiment is performed by varying the density of carriers n_s with a constant magnetic field B widths vary from $N=0$ to 3 on a vertical line corresponding to a given c_i value. Meanwhile, when experiment is given as a function of B with a constant n_s, widths are obtained for $c_i = (N+\frac{1}{2})gn_i/n_s$, where g is the degree of degeneracy. For example, for $gn_i/n_s = 0.2$, c_i varies from 0.1 to 0.7, corresponding to $N=0$ to 3. In this region Γ_0 is almost proportional to $c_i^{1/2}$, and accordingly, to l. Thus width should be proportional to l^0, or independent of B, and the peak DOS is proportional to B. For small c_i's, $\gamma_0 \propto c_i \propto l^2$ and the peak DOS is proportional to $B^{3/2}$. The experiment on the de Haas–van Alphen effect[26] gave subband widths proportional to $B^{1/2}$; this dependence is not derived on the self-consistent screening model. (According to Ref. 26 and private communications from Eisenstein, their samples have a spacer of 170 to 200 Å thick. This value is large enough and it seems to be more reasonable to assume that dopants far from the channel affect transport properties less than the imperfections within the channel, although the number of the latter is far smaller.[13] If so, the B dependence of the subband width should be analyzed in terms of short-range scattering.) For an extremely short-range potential Γ_N is known[1] to depend on l as $B^{1/2}$ and, hence, for the dependence reinterpreted in the present terminology, the same should be the case only when γ_N is given by c_i^0.

B. σ_{xx}—impurities apart from 2D EG

Considered next is the case of ionized impurities existing apart from 2D EG. The effective scattering potential

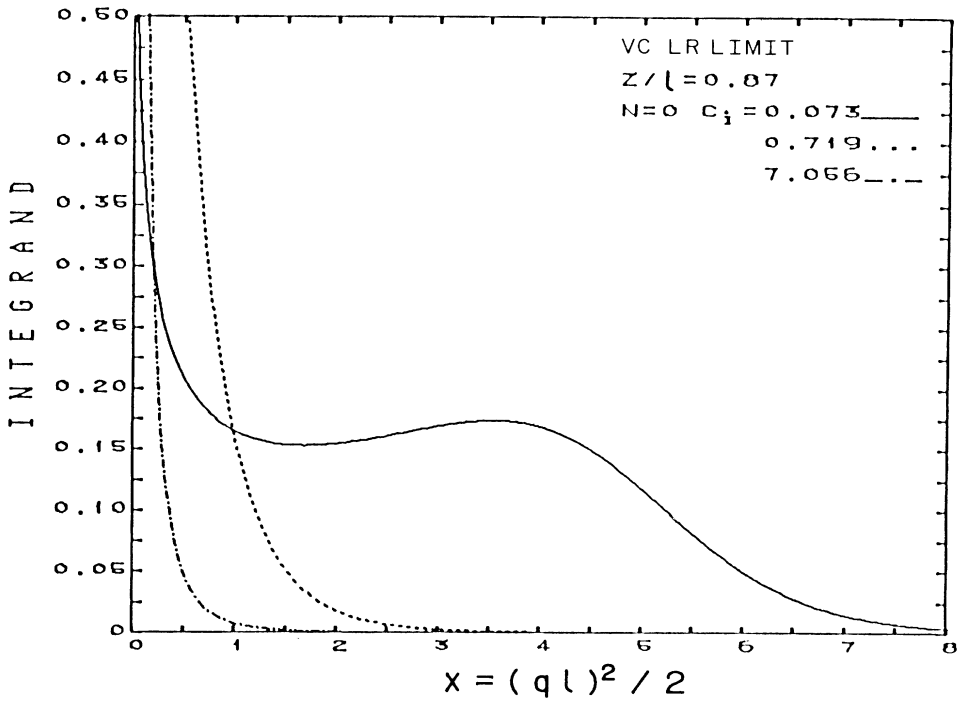

FIG. 9. Same integrands as in Fig. 7 except that impurities exist apart from 2D EG by $z_i/l = 0.87$. The solid, dotted, and dashed-dotted lines are for $c_i = 0.073$, 0.719, and 7.056, respectively.

in such devices as a modulation-doped heterostructure FET is given by Eq. (2.6) with an exponential factor, as was studied by Stern.[28] For simplicity, the doped layer is taken to be a δ-function-type sheet separated by z_i from 2D EG. It is easy to spread the dopants out across a layer of finite thickness Δz.

Since it is laborious to solve the self-consistent equation for $N \neq 0$ analytically, we perform numerical calculations. However, it may be instructive to show how the integrand runs as a function of $x=(ql)^2/2$ in Fig. 9, similarly to Fig. 7 for $z_i=0$. In Fig. 9, normalized integrands for $z_i/l=0.87$ are plotted for several c_i values, only for $N=0$. The z_i/l value corresponds to $z_i=50$ Å for $B=20$ T. It is seen that the case with a small $c_i=0.073$ has a humped region, which contributes to the integral, besides a region around $x=0$. Thus, the case behaves apparently like a short-range potential, in the meaning that potential has an appreciable magnitude throughout a finite-wavelength region. This is because when c_i is small, subbandwidth is small, which causes strong screening, and

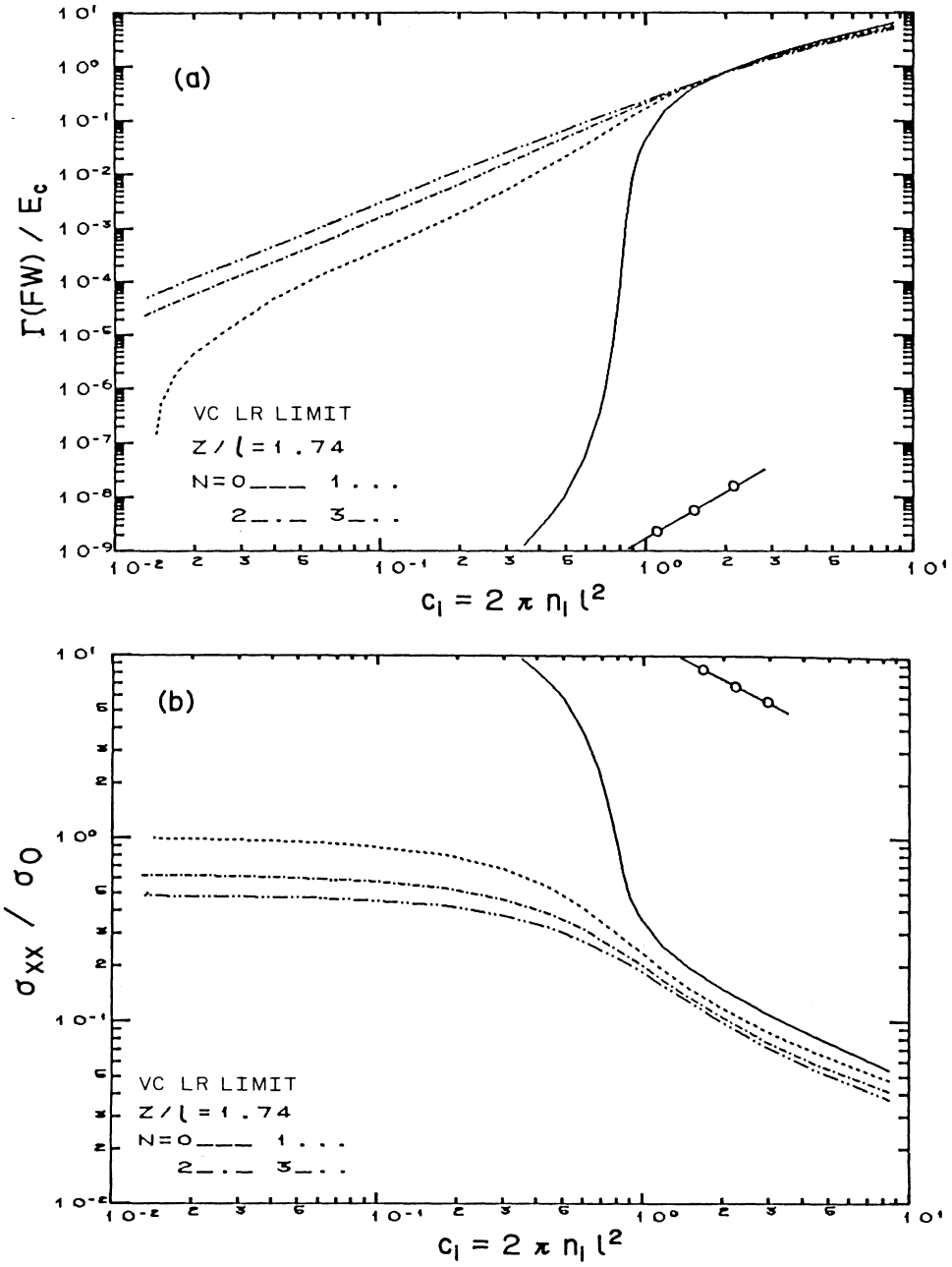

FIG. 10. (a) and (b) are the same as in Figs. 8(a) and 8(b), respectively, except for $z_i/l=1.74$. The (-0-) line is the asymptote in the narrow width limit ($c_i \ll 1$) for $N=0$.

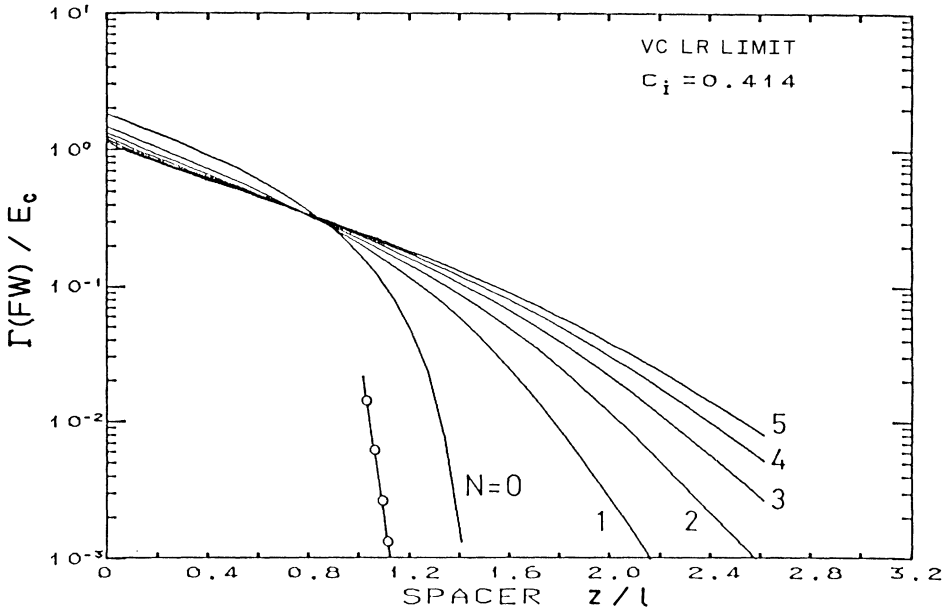

FIG. 11. Normalized full widths of subbands $2\Gamma_N/E_c$ versus thickness of spacer z_i normalized by l for $c_i=0.414$. The distribution of impurities is assumed to be like a δ function. The (-0-) line is the asymptote for $N=0$.

force range looks short.

Numerically solved results are shown in Fig. 10(a). $2\Gamma_N/E_c$ is plotted as a function of c_i for $z_i/l=1.74$. Figure 10(b) shows σ_{xx}/σ_0. In Fig. 10(a), it is remarkable that widths change drastically, as already reported in Ref. 13. This is understandable when Fig. 11 is referred to, which shows $2\Gamma_N/E_c$ as a function of the thickness of spacer z_i normalized by l.

In self-consistent screening, once a spacer is sufficiently thick, the effective scattering potential becomes sufficiently weak, which causes the width to be small and, accordingly, the screening to be effective, since screening is determined by a DOS proportional to $1/\Gamma_N$. This, in turn, makes the effectiveness of scattering potential small. Thus, a kind of positive feedback makes the width drastically small at around a finite spacer thickness of $\sim 1.2l$ for $c_i=0.414$. When $B=20$ T, the critical value is something like 80—100 Å.[13]

In terms of c_i, the situation is similar. When the z_i value is kept constant ($z_i/l=1.74$), the width is expected to be drastically reduced at a certain value of c_i; for c_i's less than the critical value, Γ_N becomes quite small. This resembles a phase transition and it occurs around $c_i=0.8$ for $N=0$ and 0.014 for $N=1$. For higher N's the same is expected to occur for much smaller c_i's.

Calculated σ_{xx} in Fig. 10(b) differs noticeably from the case with impurities within 2D EG [Fig. 8(b)]; i.e., peaks in σ_{xx} for $N=0$ are the greatest and decrease with N. This inverse order of magnitude of σ_{xx} is typical of the long-range force. In this case as well, peaks have different dependences on N, corresponding to whether an experiment is done with B or n_s as a parameter.[23] In Fig. 10 asymptotes for $N=0$ are also plotted (-0-), which expresses the solutions in the "narrow width phase."

Figure 12 shows peak values in σ_{xx} as a function of normalized spacer thickness z_i/l. The order of these peaks with N is reversed for spacer thicknesses larger than $\sim 0.5l$ when c_i is taken to be 0.414. A remarkable result is that the peak magnitudes are sufficiently large

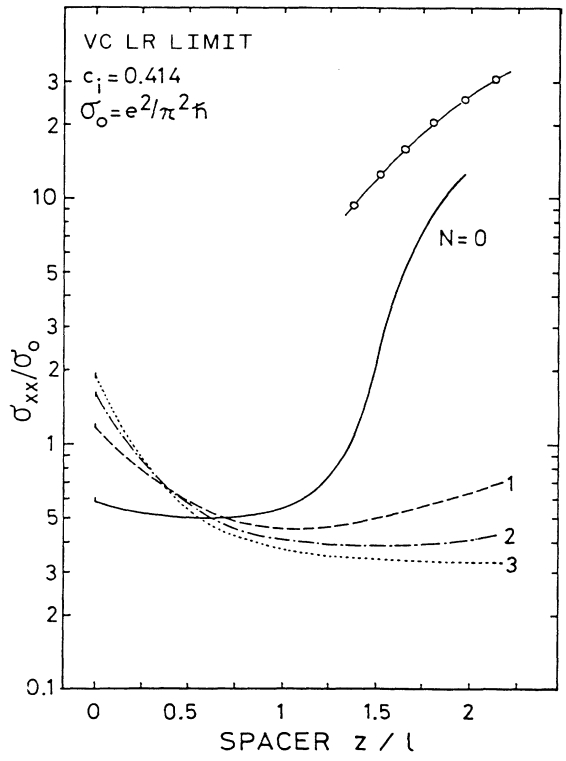

FIG. 12. Plot of peak values in σ_{xx}/σ_0 versus thickness of spacer z_i normalized by l. $c_i=0.414$.

and spread from 0.5 to 10 times σ_0 in order-of-magnitude agreement with the experiment by Narita.[18]

C. Screened potential

In the preceding sections, the self-consistent screening effect has been discussed, from which the effective Coulomb potential in its Fourier transform, $v(\mathbf{q},z_i)$, has been calculated as a function of c_i, N, and z_i. Of further interest is how the self-consistently solved potential behaves in real space.

The potential in real space, $v(\mathbf{r})$, is divided in two:

$$v(\mathbf{r})=v_0(\mathbf{r})-\Delta v(\mathbf{r}) . \tag{4.1}$$

Let us take $v_0(\mathbf{r})$ to be an unscreened part:

$$v_0(\mathbf{r})=(V_0/2\pi)\int_0^\infty dq\, J_0(qr)e^{-q|z_i|}$$
$$=(V_0/2\pi)/(r^2+z_i^2)^{1/2} , \tag{4.2}$$

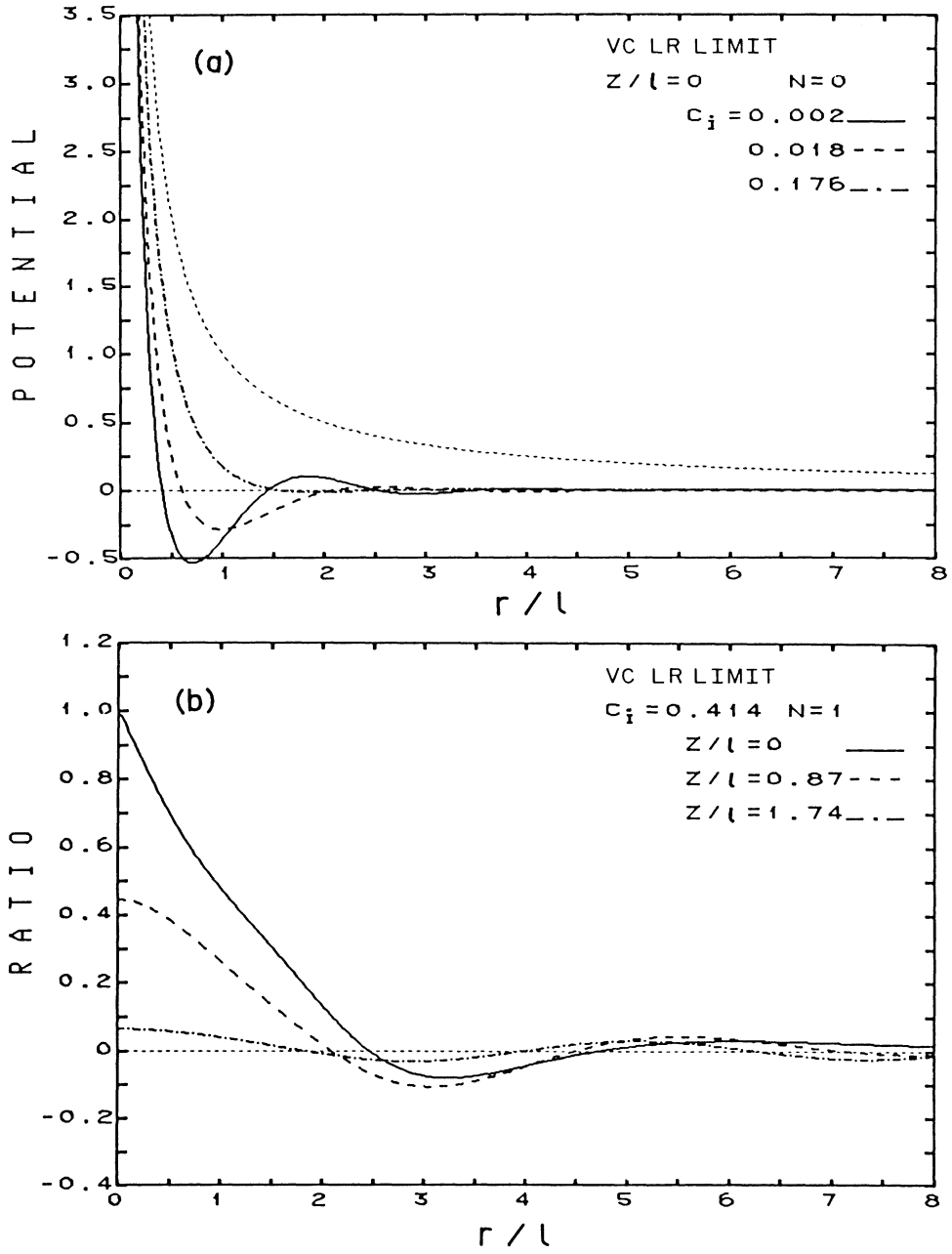

FIG. 13. (a) Potential in real space versus in-plane distance r (normalized by l) from an impurity within 2D EG ($z_i=0$). $N=0$. The solid, dotted, and dashed-dotted lines are for c_i shown in the figures, respectively. (b) The ratio $v(\mathbf{r})/v_0(\mathbf{r})$ vs r/l for $N=1$. $v(\mathbf{r})$ is the screened and $v_0(\mathbf{r})$ the *un*screened Coulomb potential. Comparisons are made among $z_i/l=0$, 0.87, and 1.74 cases.

and then

$$\Delta v(\mathbf{r}) = (V_0/2\pi) \int_0^\infty dq\, V_0 \Pi_N(q) J_0(qr) \times e^{-q|z_i|} / [q + V_0 \Pi_N(q)] \quad (4.3)$$

follows. $V_0 = 2\pi e^2/\kappa$. Figure 13(a) shows the case with impurities within 2D EG for $z_i/l = 0$. In the figure, a thin dotted line depicts $v_0(\mathbf{r})$. Only the $N = 0$ case is shown. The horizontal axis is the distance normalized by l and the vertical axis is in the unit of $e^2/\kappa l$. It is seen that potentials drop rapidly to small values around $r = l$ according to screening. The smaller the c_i is, the shorter the force range. Potentials for smaller c_i's oscillate on larger distances.

We are interested in a comparison between potentials with various z_i/l. In Fig. 13(b) three lines express the ratio $v(\mathbf{r})/v_0(\mathbf{r})$ for $N = 1$, each corresponding to $z_i/l = 0$, 0.87, or 1.74 for the same c_i value.

In the figure, the $z_i = 0$ line (the solid line) is typical. The force range, in other words, the screening length, is $2.0l$ in this case. For $z_i/l = 0.87$ (the dashed line), impurities exist apart from 2D EG at least by the value beyond a spacer; consequently, one can simulate by sketch the situation by shifting the $z_i = 0$ line by 0.87 to the left. This procedure reduces the largest part on the solid line to a smaller one, as is seen on the dashed line. For the $z_i/l = 1.74$ case, a similar procedure causes more reduction of the peak around $r = 0$. Thus, when impurities exist well apart from the channel, their potential has none of the dominant unscreened part, but only the small screened part. Accordingly, the resultant potential appears to be a roughly constant fraction of the bare Coulomb potential, and to exert a weak force similarly throughout the entire r region. This means that the potential looks long ranged, although it is highly reduced in magnitude. The long-ranged nature is more remarkable for large c_i values.

V. DISCUSSION AND CONCLUSION

The study that motivated the present authors was the Shubnikov–de Haas phenomenon observed at the heterostructure interface.[18] It showed a remarkable contrast to that observed at the Si-SiO_2 interface. The latter was successfully interpreted based on the extremely short-range scattering potential model.[1] By assuming a long-ranged Gaussian potential, it is derived that a quite different behavior is expected from that of a short-range one.[15] However, calculated transverse magnetoconductance on that Gaussian model with $d \gg l$ was too small by one or two orders of magnitude to explain experiments, although it succeeded in reproducing roughly N-independent peak values in σ_{xx}.

For a long-range $d \gg l$, a squared step on a single scattering event $(\Delta X)^2$ equals $(l^2/d)^2$ and, hence, σ_{xx}/σ_0 is given by $(l/d)^2$, except for a numerical factor of order of unity. This value is actually quite small so long as $d \gg l$ is assumed. If an experiment is performed with magnetic field as a parameter and keeping n_s (i.e., gate voltage) constant,[17,19] peaks should appear to grow roughly proportional to N, since $\sigma_{xx} \propto l^2$. This fact also seems to show the infeasibility of the Gaussian model with a constant force range.

In the present calculation the peaks are enhanced and given by $\ln(1/2\pi^2 c_i)$, due to the self-consistent treatment of screening. In order to have order-of-magnitude agreement in σ_{xx} with the observed, the self-consistent screening model seemed the most plausible. If an experiment takes magnetic field as a parameter, calculated peaks still decrease with N in our model.[23] In this paper, study is limited to the case with Fermi energy at peaks of DOS. Broadening, σ_{xx}, and cyclotron resonance width for other energies have been investigated on the same model, taking into account a more realistic distribution of impurities across a device.[13]

When Fermi energy lies around subband edges, screening is reduced due to a small DOS. This fact must force electrons to easily localize, because fluctuations due to a less screened Coulomb potential are possibly enhanced. In this situation inhomogeneous broadening surpasses collision broadening. Although in Ref. 13 broadening was calculated for energies around edges and extraordinarily broadened states were actually obtained, it lacks the viewpoint of localization, which is thought to be necessary for understanding correctly the features of the states near edges. The present work was also free from localization of Landau electrons. It is guaranteed, however, that around the peaks of subbands, electronic states are extended.[25,24] Accordingly, peaking behavior of Shubnikov–de Haas oscillations must be interpreted by considering extended states.

We have studied the effect of uncrossed vertex correction on polarizability and showed that the effect is at most $\frac{4}{3}$. Vertex correction to the self-energy of an electron as well as current vertex were also discussed by Miyake[29] using the Ward identity, by assuming that impurity potential is extremely long ranged. According to his calculation, the effect is fairly large, so long as the magneto-phonon phenomenon is concerned in a nondegenerate 3D EG system.

For a long-range potential multiple scattering is very likely to be efficient. Scattering due to many site impurities was also considered[3] in a self-consistent t-matrix approximation. Tsukada[30] and Ono[31] investigated the effect of impurity potential on Landau electrons by solving the Schrödinger equation including the potential. Crossed diagrams are considered in all these studies and they are known to highly distort the shape of Landau subbands.

According to the present study, impurities within 2D EG are well screened and the potential appears short ranged. When impurities are apart from 2D EG, the potential is to some extent screened, but the remaining part has an appreciable long-ranged feature.

It should be noted that asymptotic solution of the self-consistent equation may lose its meaning for extremely small c_i's because, there, each Landau level may generate an impurity level below and over it, not being broadened. The present solution holds true for such concentrations of impurities as to make the levels form broadened subbands. As for large c_i's, a similar problem may occur; any overlapping subbands are out of the scope of the present theory, since this is based on a single subband approximation.

Through this study we took a single subband approxi-

mation which is believed to be good for strong fields. The approximation brings a transparent view into the physics of screening. All the preceding calculations will change when screening due to multiple subband structure is taken into account. If a specific N is of concern, polarizability is composed of Π_N and $\sum_{N'(\neq N)}\Pi_{NN'}$. The latter is roughly smaller than the former by a factor of $1/\omega_c\tau$. It is obvious that Π_N is the most dominant so long as ε_F stays around the Nth peak. However, for large $x=(ql)^2/2$, $\Pi_{NN'}$ becomes more effective, since

$$\Pi_{NN'} \propto [J_{NN'}(x)]^2 \propto x^{|N-N'|}\exp(-x) .$$

This causes the hump in Fig. 7 to be relatively reduced for small c_i's. Thus, the inclusion of other subbands in screening will make the scattering feature appear more long ranged. In other words, peaks in σ_{xx} will be reduced for small c_i's and will become less sensitive to N. For an extremely short-range force the inclusion of multiple subbands was rather an easy matter, because damping $\mathrm{Im}\,\Sigma_N(E)$ was independent of N therein.[1] However, in our case, it is a tedious process to take a number of subbands and make consistent their widths and polarizabilities due to so many subbands.

Every calculation was performed in a normalized form, irrespective of specific material constants. Therefore, all the results can be applied to both Si MOS and GaAs heterostructure FET's as well. This means that if the same kind of impurity distribution occurs in the Si-SiO_2 interface, the system would develop such a Shubnikov–de Haas effect as was calculated in the present work. The actual Si-SiO_2 system is believed to have dominant ionized impurities just at the interface. Measurements in that system also agree qualitatively with the present results when impurities are taken to exist within 2D EG, but not quantitatively; calculated peaks in σ_{xx} are quite larger than the observed.

In summary, self-consistent screening between widths of Landau subbands and polarizability was discussed, and it has been shown that the states thus solved can really simulate successfully the behavior of peaks in σ_{xx} at the heterostructure interface, which is quite different from what is seen at the Si-SiO_2 interface. Numerical as well as asymptotically analytical solutions of self-consistent equations were obtained. Calculations were made on widths of Landau subbands and on peak values in σ_{xx}, as well as on screened Coulomb potentials in real space.

ACKNOWLEDGMENTS

The authors are grateful to Professor S. J. Miyake for his valuable discussions. This work is partially supported by a Grant-in-Aid for Special Promotion of Science by the Ministry of Education, Culture and Science, Japan.

APPENDIX A

Let $\mathscr{V}$ and $\mathscr{G}$ be temperature Green's functions for the vertex part and propagator, respectively. Then

$$\mathscr{V}_{NX,N'X'}(\varepsilon-\omega,\varepsilon;\mathbf{q}) = J_{NN'}(q) + k_BT\sum_{\omega'}\sum_{N'',N''',\mathbf{q}'}(n_i/L^2)\mathscr{V}_{N''X+l^2q_y',N'''X'+l^2q_y'}(\varepsilon-\omega-\omega',\varepsilon-\omega';\mathbf{q}) \times \exp[-il^2(\mathbf{q}_x'\cdot\mathbf{q}_y-\mathbf{q}_x\cdot\mathbf{q}_y')+i[N'''-N''-N'+N](\phi-\phi')] \times |v(\mathbf{q}',z)|^2 J_{NN''}(q')J_{N'N'''}(q')\mathscr{G}_{N''}(\varepsilon-\omega-\omega')\mathscr{G}_{N'''}(\varepsilon-\omega') \quad (A1)$$

is obtained, where $\phi=\arctan(\mathbf{q}_y/\mathbf{q}_x)$ and $\phi'=\arctan(\mathbf{q}_y'/\mathbf{q}_x')$. After replacing $\sum_{\mathbf{q}'}$ by $(L/2\pi)^2\int q'dq'\int d\phi'$ and calculating the integral, a Bessel function $2\pi J_{N'-N+N''-N'''}(l^2qq')$ results. If only the Nth subband is of concern, we are left with $J_0(l^2qq')$, as seen in Eq. (2.8).

APPENDIX B

For readers' convenience we reproduce here

$$\langle|\langle NX|U(\mathbf{r})|N'X'\rangle|^2\rangle_S=(n_i/L^2)\sum_{q_xq_y}|v(\mathbf{q},z)|^2J_{NN'}(X,q_x,X')J_{NN'}(X,-q_x,X')\delta_{q_y,(X-X')/l^2} , \quad (B1)$$

where

$$J_{NN'}(X,q_x,X')=\exp(-|\kappa|^2/2)\times\begin{cases}(N'!/N!)^{1/2}(-\kappa)^{N-N'}L_{N'}^{(N-N')}(|\kappa|^2), & \text{for } N\geq N'\\ (N!/N'!)^{1/2}(\bar{\kappa})^{N'-N}L_N^{(N'-N)}(|\kappa|^2), & \text{for } N\leq N'\end{cases} \quad (B2)$$

with $|\kappa|^2=\kappa^2=\kappa_x^2+\kappa_y^2=(lq_x/\sqrt{2})^2+[(X-X')/\sqrt{2}l]^2$, and $L_p^{(q)}$ is the associated Laguerre polynomial of rank (p,q).[32] For $\mathbf{q}=(\mathbf{q}_x,(X'-X)/l^2)$ it is easy to obtain

$$(2\pi)^{-2}\int J_{NN'}(q)^2e^{i\mathbf{q}\cdot\mathbf{r}}d\mathbf{q}=[1/2\pi l^2]J_{NN}(0,\bar{y}/l^2,\bar{x})J_{N'N'}(0,\bar{y}/l^2,\bar{x}) , \quad (B3)$$

where $\bar{x}=l^2\mathbf{q}_x$ and $\bar{y}=l^2\mathbf{q}_y$. Thus

$$(2\pi)^{-2}\int d\mathbf{k}\,J_{NN}(k)^2\exp(i\mathbf{k}\times\mathbf{q}l^2)=[J_{NN}(q)]^2/2\pi l^2 \quad (B4)$$

was proved.

[1]T. Ando and Y. Uemura, J. Phys. Soc. Jpn. **36**, 959 (1974).
[2]T. Ando, J. Phys. Soc. Jpn. **36**, 1521 (1974).
[3]T. Ando, J. Phys. Soc. Jpn. **37**, 622 (1974).
[4]T. Ando, J. Phys. Soc. Jpn. **37**, 1233 (1974).
[5]T. Ando, A. B. Fowler, and F. Stern, Rev. Mod. Phys. **54**, 437 (1982).
[6]M. E. Rensink, Phys. Rev. **174**, 744 (1968).
[7]M. L. Glasser, Phys. Rev. **180**, 942 (1969); Can J. Phys. **48**, 1941 (1970).
[8]N. J. Horing, Phys. Rev. **186**, 434 (1969).
[9]T. Ando and Y. Uemura, J. Phys. Soc. Jpn. **37**, 1044 (1974).
[10]T. Ando, J. Phys. Soc. Jpn. **43**, 1616 (1977).
[11]S. Das Sarma, Phys. Rev. B **23**, 4592 (1981).
[12]R. Lassnig and E. Gornik, Solid State Commun. **47**, 959 (1983).
[13]T. Ando and Y. Murayama, in *Proceedings of the 17th International Conference on Physics of Semiconductors, San Francisco, 1984,* edited by J. D. Chadi and W. A. Harrison (Springer, New York, 1986), p. 317; J. Phys. Soc. Jpn. **52**, 1519 (1985).
[14]W. Cai and C. S. Ting, Phys. Rev. B **33**, 3967 (1986).
[15]Y. Murayama (unpublished).
[16]T. Ando, Y. Matsumoto, Y. Uemura, M. Kobayashi, and K. F. Komatsubara, J. Phys. Soc. Jpn. **32**, 859 (1972).
[17]S. Kawaji and J. Wakabayashi, Surf. Sci. **58**, 238 (1976).
[18]S. Narita, Butsuri **37**, 837 (1981) (in Japanese); S. Narita, S. Takeyama, W. B. Luo, S. Hiyamizu, K. Nambu, and H. Hashimoto, J. Phys. Soc. Jpn. **20**, L443 (1981); Surf. Sci. **113**, 301 (1982).
[19]K. von Klitzing, *Festkörperprobleme,* Vol. 21 of *Advances in Solid State Physics,* edited by J. Treusch (Vieweg, Braunschweig, 1981), p. 1; Surf. Sci. **113**, 1 (1982).
[20]Y. Guldner, J. P. Hirtz, J. P. Vieren, P. Voisin, M. Voss, and M. Razeghi, J. Phys. (Paris) Lett. **43**, L613 (1982).
[21]R. Kubo, H. Hasegawa, and N. Hashitsume, J. Phys. Soc. Jpn. **14**, 56 (1959).
[22]R. Kubo, S. J. Miyake, and N. Hashitsume, in *Solid State Physics,* edited by F. Seitz and D. Turnbull (Academic, New York, 1965), Vol. 17, p. 269.
[23]Y. Murayama and T. Ando, Proceedings of the Yamada Conference on Electronic Properties of Two-dimensional Systems, Kyoto, 1985 [Surf. Sci., **170**, 311 (1986)].
[24]Y. Ono, J. Phys. Soc. Jpn. **51**, 2055 (1982); **52**, 2493 (1983).
[25]T. Ando, Surf. Sci. **113**, 182 (1982); J. Phys. Soc. Jpn. **52**, 1740 (1983).
[26]J. P. Eisenstein, H. L. Stormer, V. Narayanamurti, A. Y. Cho, C. Gossard, and C. W. Tu, Phys. Rev. Lett. **55**, 875 (1985); Proceedings of the Yamada Conference on Electronic Properties of Two-dimensional Systems, Kyoto, 1985 [Surf. Sci. **170**, 271 (1986)]; (private communications).
[27]A. A. Abrikosov, L. P. Gorkov, and I. E. Dzyaloshinski, *Methods of Quantum Field Theory in Statistical Physics* (Dover, New York, 1961).
[28]F. Stern, Phys. Rev. Lett. **18**, 546 (1967).
[29]S. J. Miyake, J. Phys. Soc. Jpn. **46**, 377 (1979); (private communication).
[30]M. Tsukada, J. Phys. Soc. Jpn. **41**, 1466 (1976).
[31]Y. Ono, J. Phys. Soc. Jpn. **51**, 237 (1982).
[32]S. Moriguchi *et al., Mathematical Formulas* (Iwanami, Tokyo, 1956) (in Japanese).